SANDIA REPORT

SAND201X-XXXX
Unlimited Release
Printed Month and Year

Microfabricated Waveguide Atom Traps

Yuan-Yu Jau and Jongmin Lee

Prepared by
Sandia National Laboratories
Albuquerque, New Mexico 87185 and Livermore, California 94550

Sandia National Laboratories is a multimission laboratory managed and operated by National Technology and Engineering Solutions of Sandia, LLC, a wholly owned subsidiary of Honeywell International, Inc., for the U.S. Department of Energy's National Nuclear Security Administration under contract DE-NA0003525.

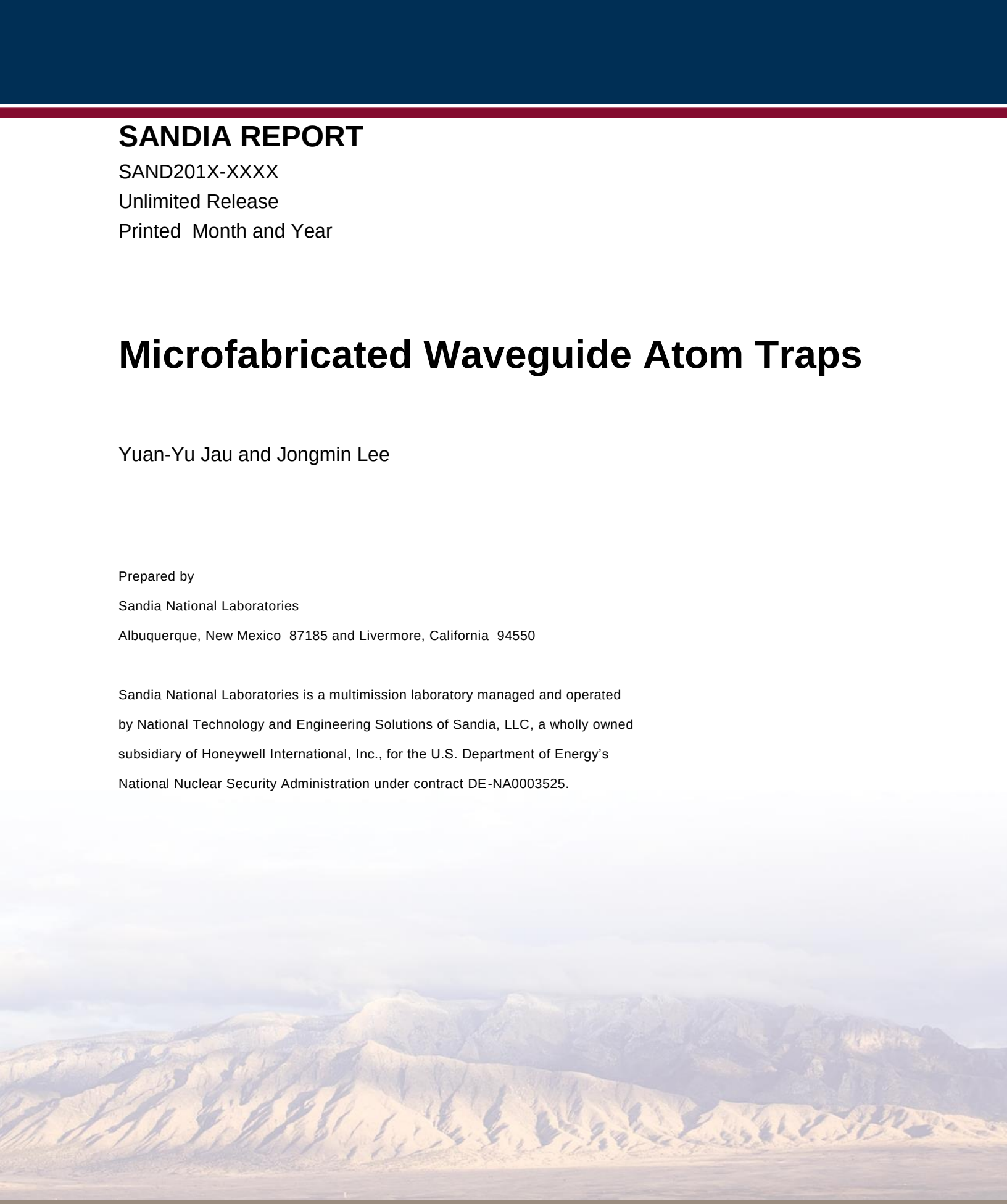

Issued by Sandia National Laboratories, operated for the United States Department of Energy by National Technology and Engineering Solutions of Sandia, LLC.

Available to DOE and DOE contractors from
U.S. Department of Energy
Office of Scientific and Technical Information
P.O. Box 62
Oak Ridge, TN 37831

Telephone: (865) 576-8401
Facsimile: (865) 576-5728
E-Mail: reports@osti.gov
Online ordering: http://www.osti.gov/scitech

Available to the public from
U.S. Department of Commerce
National Technical Information Service
5301 Shawnee Rd
Alexandria, VA 22312

Telephone: (800) 553-6847
Facsimile: (703) 605-6900
E-Mail: orders@ntis.gov
Online order: https://classic.ntis.gov/help/order-methods/

SAND201X-XXXX
Printed September 2017
Unlimited Release

Microfabricated Waveguide Atom Traps

Yuan-Yu Jau and Jongmin Lee
Org. 05228 Physics-Based Microsystems
Sandia National Laboratories
P. O. Box 5800
Albuquerque, New Mexico 87185-MS1082

Abstract

A nano-scale, microfabricated waveguide structure can in-principle be used to trap atoms in well-defined locations and enable strong photon-atom interactions. A neutral-atom platform based on this microfabrication technology will be pre-aligned, which is especially important for quantum-control applications. At present, there is still no reported demonstration of evanescent-field atom trapping using a microfabricated waveguide structure. We described the capabilities established by our team for future development of the waveguide atom-trapping technology at SNL and report our studies to overcome the technical challenges of loading cold atoms into the waveguide atom traps, efficient and broadband optical coupling to a waveguide, and the waveguide material for high-power optical transmission. From the atomic-physics and the waveguide modeling, we have shown that a square nano-waveguide can be utilized to achieve better atomic spin squeezing than using a nanofiber for first time.

ACKNOWLEDGMENTS

We are grateful to Dr. Grant Biedermann, Dr. Erica Douglas, Dr. John Mudrick, Dr. Matt Eichenfield and Dr. Aleem Siddiqui for their contributions to this project. We would like to thank Mr. Xiaodong Qi (UNM graduate student) and Prof. Ivan Deutsch (UNM) for their quantum theory work contributing to this project. We are also grateful to Dr. Mary Crawford for her support to this research project.

TABLE OF CONTENTS

FIGURES

TABLES

No table of figures entries found.

NOMENCLATURE

Abbreviation	Definition
AMO	Atomic, molecular, and optical
ATC	Adiabatic transfer coupling
HEPA	High-efficiency particulate air
MFD	Mode field diameter
MOT	Magneto-optical trap
NIR	Near Infrared
PC	Photonic crystal
PZT	Lead zirconate titanate
QED	Quantum electrodynamics
Sandia	Sandia National Laboratories
SNL	Sandia National Laboratories
SWG	Square waveguide
TE	Transverse electric
TM	Transverse magnetic
UV	Ultraviolet
WG	Waveguide

1. Introduction

Ultra-cold gaseous atomic samples formed through laser cooling and trapping provide a foundation for implementing quantum computing and communication technologies and for performing precision measurements (quantum sensing) such as inertial sensing, magnetometry, and time keeping. However, the laboratory trapping and probing technology has proven difficult, inhibiting the transition into practical applications. Hence, an alignment-free, cold-atom platform is desirable. One potential route is to develop a new type of "optical atom chip" by engineering the evanescent light fields of microfabricated structures, such as suspended optical nano-waveguides, to trap and control neutral atoms. Since all the trap, probe, and control optical fields are guided through a waveguide structure, it naturally eliminates the need of complex, free-space laser alignments. This is especially beneficial when multiple atom traps are required. Furthermore, the entire neutral-atom platform is microfabricated, it is therefore in-principle expandable. A novel and important benefit to trapping the atoms in the evanescent field of a waveguide is that both the trapped atoms and photons traveling through the waveguide are confined within a very small region of space (sub-micron) creating strong photon-atom interactions. This leads to a high ratio of σ_0/A_{eff}, where σ_0 is the photon scattering cross section of trapped atoms, and A_{eff} is the effective laser intensity area. It is well known that the photon-assisted quantum-control strength, $\mathcal{F} \cdot \sigma_0/A_{\text{eff}}$, is the key for demonstrating cavity-QED effect, cavity-enhanced spin squeezing, and quantum optimal controls. Here, $\mathcal{F}$ is the cavity finesse. Hence, strong photon-atom interactions are crucial to many schemes for quantum sensing and quantum information processing. Generally, a nano-waveguide neutral-atom platform can achieve a value of σ_0/A_{eff} 1000x better than a neutral-atom system implemented in free space. By incorporating a specific photonic-crystal structure to a waveguide, the effective σ_0/A_{eff} can be even larger, and the control can be more adjustable. With this significant enhancement, various quantum controls can be greatly improved. Therefore, the waveguide-based neutral-atom platform is highly attractive for development.

The waveguide-based atom-trap platform was originally proposed in early 2000 [1-2]. After the demonstration of evanescent-field atom trapping using an optical nanofiber in 2010 [3] and in 2012 [4], research groups in Caltech[5], Harvard, JQI[6], NRL, Purdue University[7], etc. conducted extensive work to realize neutral-atom platforms based on microfabricated structures. Impeded by various technical challenges, evanescent-field trapping using a microfabricated structure has still not been demonstrated. An alternative approach was published and described in Ref.[8-9]. Reviewing the work from Ref.[9], a free-space laser beam was required to produce near-surface interference fringes adjacent to the microfabricated structure. Atoms are trapped in the high-

intensity regions of the fringes. Because of this special implementation, up to about three atoms were able to be trapped. However, the trapped atoms were not close enough to the photonic-crystal waveguide, and therefore it was difficult to overlap the trapped atom with the desired optical-field mode to achieve strong photon-atom interactions. There are proposed ideas [7] to improve the scalability and the photon-atom interaction strength along with this approach. Still, enabling evanescent-field trapping will be the best option to reduce the complexity of the optical atom chip if the technical challenges can be overcome.

There are several identified technical issues for developing microfabricated waveguide atom traps. The major problem is that the microfabricated suspended waveguide cannot handle the required optical power, which is ~ 10 mW in vacuum, to provide sufficient depth in the evanescent-field trap. The unwanted optical loss in the microfabricated waveguide or photonic-crystal structure causes heat generation that destroys the device. Such problems may occur during the fabrication process or with atomic adsorption to the waveguide material. On the other hand, a tapered optical fiber to a sub-micron diameter can easily handle optical power up to several hundred mW in vacuum. In addition, production of cold atoms and the constant atomic cooling force at the waveguide atom traps are important to efficiently load atoms into relatively weak evanescent-field trapping potential. For a large-scale system, economic use of laser power for trapping atoms is desired. For quantum controls, high-fidelity readout and control of the atomic states are necessary. Hence, it is important to develop broadband and high-efficiency optical coupling schemes between the waveguides and the optical fibers. Later, after succeeding with evanescent-field trapping, waveguide modeling and the associated atomic-physics modeling will allow us to achieve the best control for a specific quantum application.

For future development of neutral-atom quantum technology at SNL, we have carried out research work to address several technical challenges of waveguide atom traps and established essential capabilities toward on-chip neutral-atom quantum controls.

2. Modeling work for waveguide atom traps

For developing a neutral-atom platform based on microfabricated waveguides and photonic-crystal structures, we have developed modeling capabilities for designing the photonic structures and for the associated atomic physics regarding cooling, atom trapping and probing, and controlling the atomic states.

2.1. Full-level atomic-physics modeling

In order to optimize the control and access of the atomic state and to achieve atom cooling and trapping of atoms with a waveguide or photonic-crystal structure, detailed models are required. This enables us to design the system in the way we would like the atoms to affect photons propagating through a waveguide and to be cooled, trapped, and controlled by the optical fields. For these purposes, we developed numerical models in Matlab based on density-matrix formalisms[10] with all required atomic levels. For example, Fig. 1 plots the energy shifts of the all sublevels of ^{133}Cs $6S_{1/2}$ and $6P_{3/2}$ states associated with the optical polarizations. Such calculation is especially important when we need to know how the local optical fields affect the atomic levels of interest and how the optical pumping, probing, or cooling transition is influenced by other optical fields at the atom. The so-called "magic wavelengths," which do not perturb the $S_{1/2}$—$P_{3/2}$ cooling transition, are found at the blue circles in Fig. 1. They are 686 nm, 793 nm, 886 nm for blue-detuned light and 921 nm, 937 nm for red-detuned light. With a closer look, one can see that $|F' = 5, |m| = 5\rangle$ sublevels do not cross over the $6S_{1/2}$ curve when the local optical field is π-polarized around 793 nm. So this wavelength is not truly "magic."

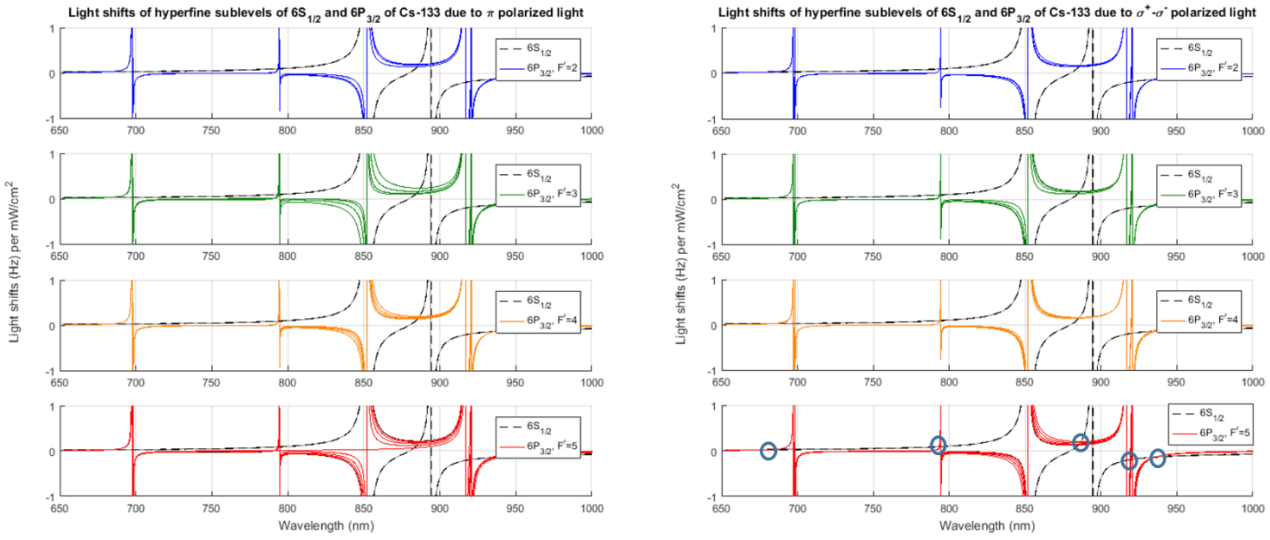

Figure 1. Shifts of ^{133}Cs energy levels as functions of optical wavelength

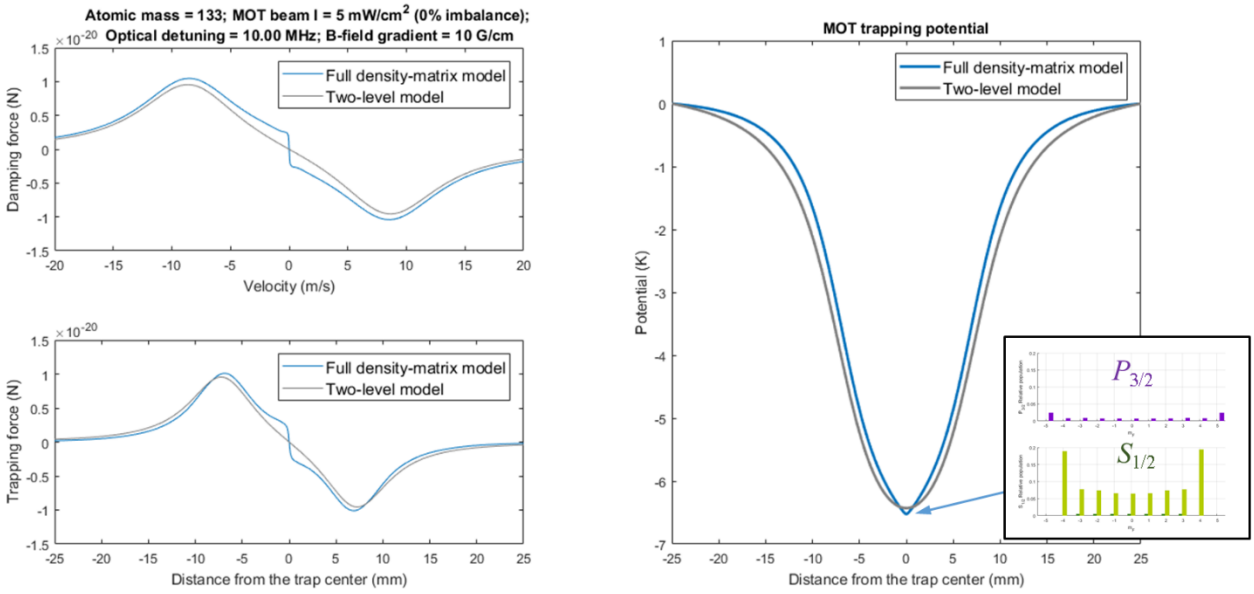

Figure 2. Full-level modeling of a ^{133}Cs MOT.

The advantage of conducting full-level modeling can be shown from another example in Fig.2. The simple two-level modeling can explain the phenomena of cooling and trapping of atoms qualitatively. However, when a more accurate description of the dynamics of atoms in a magneto-optical trap (MOT) is needed, we need to include all the associated energy sublevels into the calculation. Figure 2 shows that the velocity-dependent damping of a ^{133}Cs atom is much stronger at very low velocity [10], and the position-dependent trapping force is also much sharper near the trap center. The steady-state relative populations of the atomic sublevels at the MOT center is shown in the inset of Fig. 2. All of this information detail cannot be obtained by using two-level modeling.

2.2. Evanescent-field trapping potential modeling with Casimir-Polder Effect

To model the light propagation through a regular or photonic-crystal waveguide and the effect of the presence of atoms near the structure, we take the advantage of commercial software including COMSOL, Lumerical, FIMMWAVE, and OmniSim. With the given material properties, dimension, and the geometry of the waveguide and the surrounding materials and configurations, we can calculate different propagation modes, optical-field distribution with polarization information, coupling efficiency between different structures, the effect of near-surface electric dipoles, etc.

In Fig.3, we shows the calculated trap volumes (purple-blue regions) for ^{133}Cs atoms by running 686-nm and 937-nm light with specific optical power through different SiN waveguide geometry. The optical electric fields are calculated numerically with commercial software. The trapping

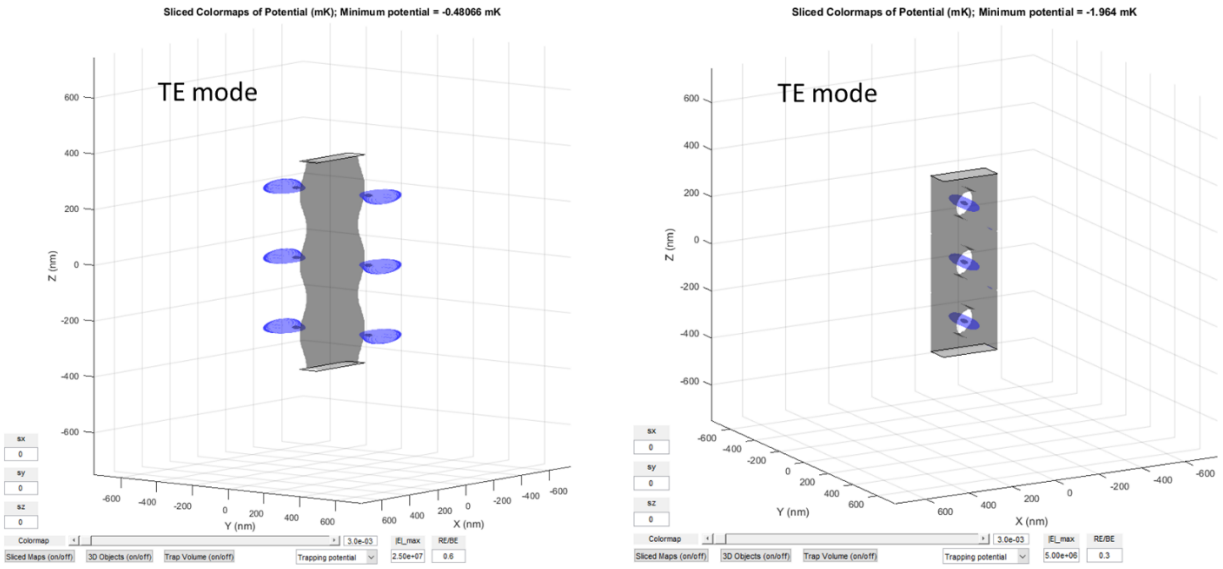

Figure 3. Different waveguide geometry and atom trap volumes

potentials are calculated in Matlab for inspection and visualization. In addition to the evanescent-field trapping potential, since the atom trapping sites are very close (~ 100 nm) to the waveguide structure, we also need to consider the Casimir-Polder effect, which leads to attractive force from the atom toward the nearby surface. We developed numerical codes in Matlab to calculate the Casimir-Polder effect. In Fig. 4, we look at one section of a photonic-crystal waveguide with periodic holes. The trap volume is inside the hole, and we find the optical trapping potential plotted as blue curves along the three orthogonal axis intercepted at the trap center. The red curves

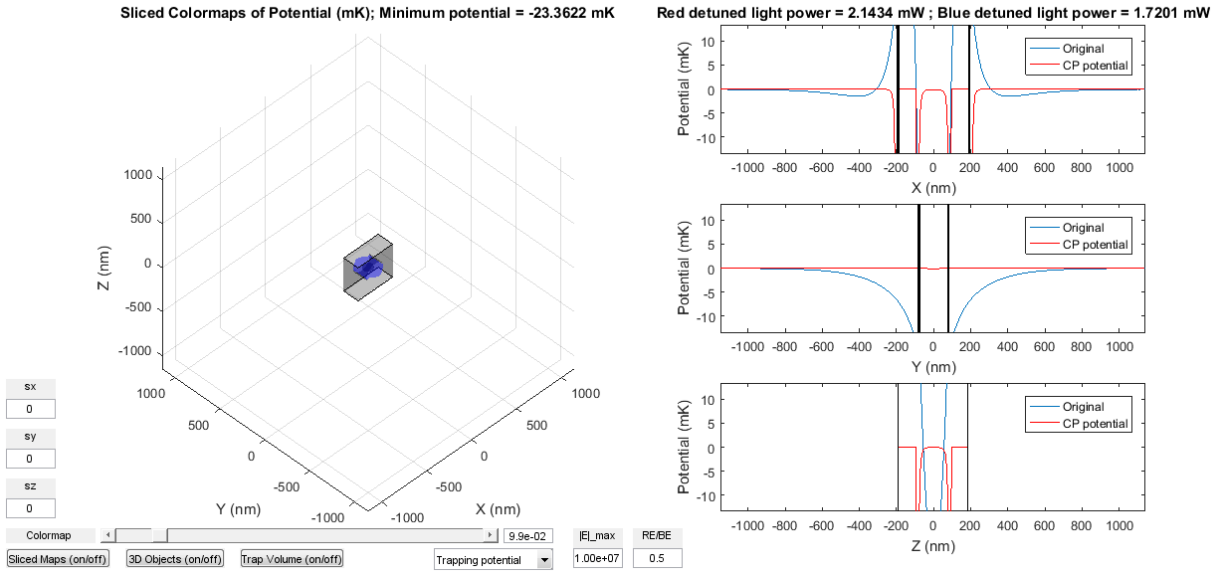

Figure 4. Trapping potential + Casimir-Polder potential

represents the calculated Casimir-Polder potential. Depending on how much repulsive force can be generated from the blue-detuned optical evanescent field, normally the Casimir-Polder force becomes very pronounced when the distance from the nearby surface is shorter than 50 nm.

3. Tapered-fiber pulling systems

Optically interfacing the waveguide and PC devices for achieving a practical optical atom chip is crucial. One option is to use micron or sub-micron tapered optical fiber to couple the light between the microfabricated devices and the regular optical fibers. Furthermore, the optical nanofiber has shown evanescent-field trapping capability and can provide similar evanescent-field conditions that can allow us to do some experimental studies to simulate waveguide atom traps. We have set up two different optical nanofiber pulling systems for this research project and another on-going project at Sandia for guided atom interferometry.

3.1. 1st tapered-fiber puller

The tapered fiber pulling stage was originally set up inside a HEPA filtered environment (the left

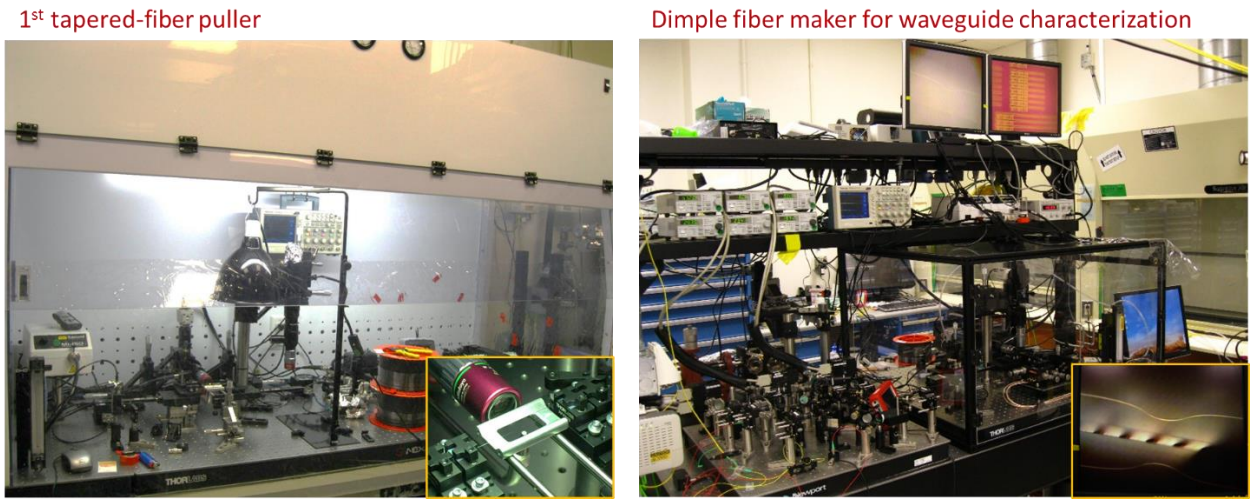

Figure 5. 1st fiber puller and dimpled fiber maker

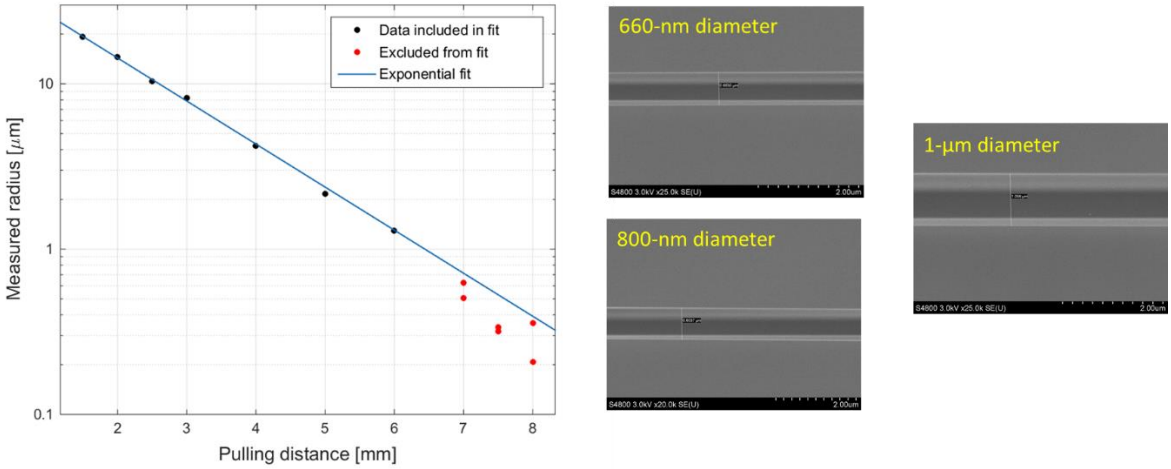

Figure 6. Reliability of fiber pulling from 1st fiber puller system

picture in Fig.5). The system is based on 25mm one-axis motorized translation stages (Thorlabs PT1-Z8, 29nm minimum resolution) and H2 flame, which can fabricate an exponentially tapered, micron-diameter fiber using a linear pulling process. We are able to reliably fabricate 1 to 1.2μm diameter tapered fiber after 15mm each fiber pulling with ~80% light transmission. However, for tapered fiber diameter below 1 μm, the reproducibility becomes poor as shown in Fig.6. In the system, the flow rate of H_2 flame for heating up the fiber is well controlled by an OMEGA flow meter, and the optimal position and flow rate of H_2 flame must be found by several experimental trial pulling. The flow rate and the position of the flame are important factors for reliable fiber pulling together with a fiber cleaning process. After removing a fiber buffer layer with a mechanical fiber stripper, we clean the fiber surface (cladding) multiple times by clean-room wipes (Texwipe ThermoSeal60: TX2064, 4''x4'') with acetone and methanol and inspect the surface through an objective lens. A blunted fiber stripper needs to be replaced with a new one every time, because it lets some residue remained on the surface after the cleaning process. Residues on the surface become critical defects to terminate the fiber pulling process due to heat.

This micron-diameter tapered-fiber puller was later moved to a larger clean-room environment and converted to a dimpled fiber maker for waveguide characterization as shown in the right picture in Fig.5. The example dimpled fiber picture is shown in the inset picture. In general, a micron-diameter dimpled tapered fiber is enough to couple a telecom wavelength light (1560nm) to telecom photonic devices, but it is not straightforward to couple near-infrared (NIR) wavelength light (685nm, 852nm, 938nm for ^{133}Cs) to NIR WGs due to a shorter wavelength. Therefore, the yield rate of a micron-diameter dimpled tapered fiber for the evanescent-field WG coupling decreases at NIR wavelengths. Because of the surface interaction between a tapered fiber and particles in air, the transmission of a tapered fiber degrades as time goes on. It is required to process the WGs and then to transferring the tapered fiber (glued on a U-mount) to the vacuum chamber.

3.2. New advanced tapered-fiber puller

The capability of transmitting optical power through a micron-diameter tapered fiber in vacuum can be more than 50mW which is enough to trap atoms in vacuum, and we can always see thermal neutral atoms with the fiber probe. However, the diameter uncertainty and the small evanescent-field mode of an exponentially tapered, micron-diameter fiber fabricated by linear pulling process makes it difficult to trap and detect cold atoms through the fiber in vacuum. The uncertainty of its diameter limits a sub-micron-diameter tapered fiber due to the minimum resolution of linear motors, no algorithmic control of pulling process, and the instability of H_2 flame. The linear pulling process with a velocity and an acceleration is only capable of creating an exponentially tapered

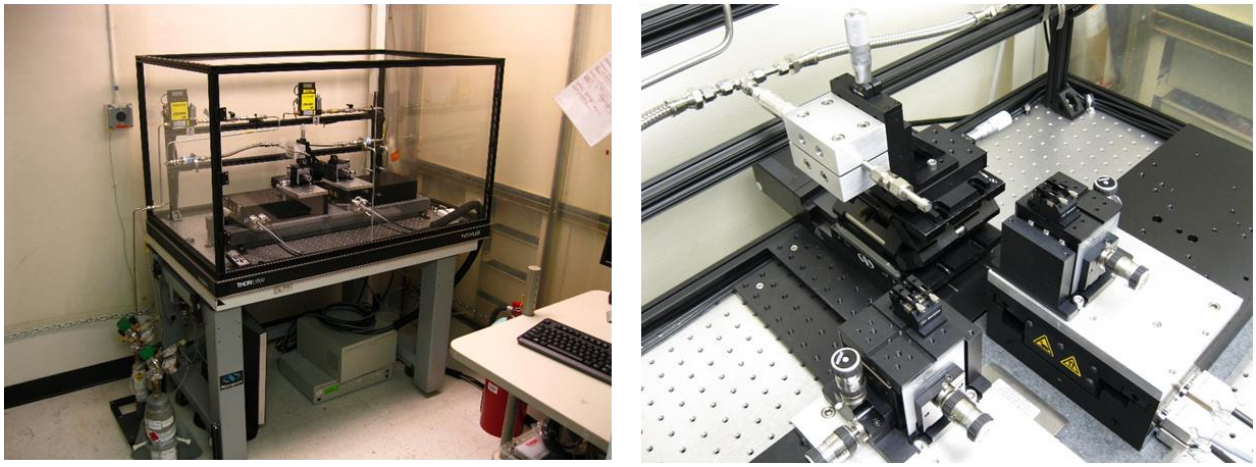

Figure 7. Advance tapered-fiber pulling system

fiber which is longer, mechanically not robust, with lower transmission, and is less adiabatic than a linear-to-exponential taper fiber with algorithmic pulling. Resolution of a few nanometers is required for algorithmic pulling.

To achieve reliable sub-micron tapered-fiber pulling, we have set up an advanced puller system in a clean-room environment as shown in Fig.7. This system uses the same design as the one developed in the University of Maryland [11]. The fabrication of a sub-micron-diameter tapered fiber requires algorithmic pulling, two nanometer resolution linear motors, and stable H_2/O_2 flame. This flame does not require air and Oxygen is more controllable with a flow meter. Thus, this could be more stable than H_2 flame. We are using two Newport XML210 linear motors with 1nm minimum resolution. Its MultiAxesPVT mode allows two motors to move based on a uploaded PVT trajectory file which is created from an algorithm pulling code and is composed of [Delta Time, Position1, Velocity 1, Position2, Velocity 2]. Two linear motor stages has been installed on a granite base to obtain the minimized surface variation and reduce some motional vibration created from motors. Two stages move back and forth together around the H_2/O_2 flame, pulling a fiber a bit more when the motor stages reach each endpoint. The torch tip is custom designed to have an array of small venting holes. The algorithmic pulling process (with adjustable velocities and accelerations) leads to a linear-to-exponential fiber taper, which is shorter, mechanically robust, and has a higher transmission (more than 95%), and more adiabatic, than an exponentially tapered fiber with linear pulling of a fixed velocity and acceleration. Currently, the system has been built up with H_2/O_2 flame in clean room and the fiber-pulling system is working with algorithmic pulling. We expect to use this setup for fabricating a better dimpled tapered fiber which has higher transmission with more adiabatic tapers and mechanically reliable, short tapers. Although there was not enough time to utilize this sub-micron tapered-fiber puller, a continuing project for a guided atom interferometer will inherit this system and take advantage of it.

4. Fabrication of suspended waveguide devices

Sandia has an in-house microfabrication capability and has previously fabricated many waveguide and photonic-crystal devices. However, those microfabricated devices were primarily designed for telecom applications at wavelengths near 1.55 µm. There were few cases targeting at wavelength below 1 µm. For waveguide atom-trapping technology developed at Sandia, we need to establish the microfabrication capability of suspended photonic-crystal waveguides with good optical quality for wavelengths ranging from 600 nm to 1000 nm. In particular, we explored not only silicon nitride (SiN) but also aluminum nitride (AlN) materials for making the waveguide devices. Although SiN has been the main microfabrication material used in the AMO research work, after years of investigation by different research groups, microfabricated SiN suspended waveguides have shown incapable of handling the required optical power for evanescent-field trapping. AlN material, on the other hand, has similar optical properties and mechanical strength compared to SiN material. Most importantly, AlN has 10x—20x higher thermal conductivity than SiN. With this, we may be able to deliver sufficient optical intensity to trap atoms without destroying the suspended waveguide. Furthermore, crystalline AlN has electro-optic and piezo effects. This enables capabilities of tuning the waveguides electrically or tuning by mechanical methods.

4.1. High optical quality SiN and AlN membranes

Fabricating suspended waveguides or photonic-crystal structures requires membrane materials (a few hundred nm thick) with good initial optical quality. After a few fabrication iterations, we have developed processes to make good SiN and AlN membranes.

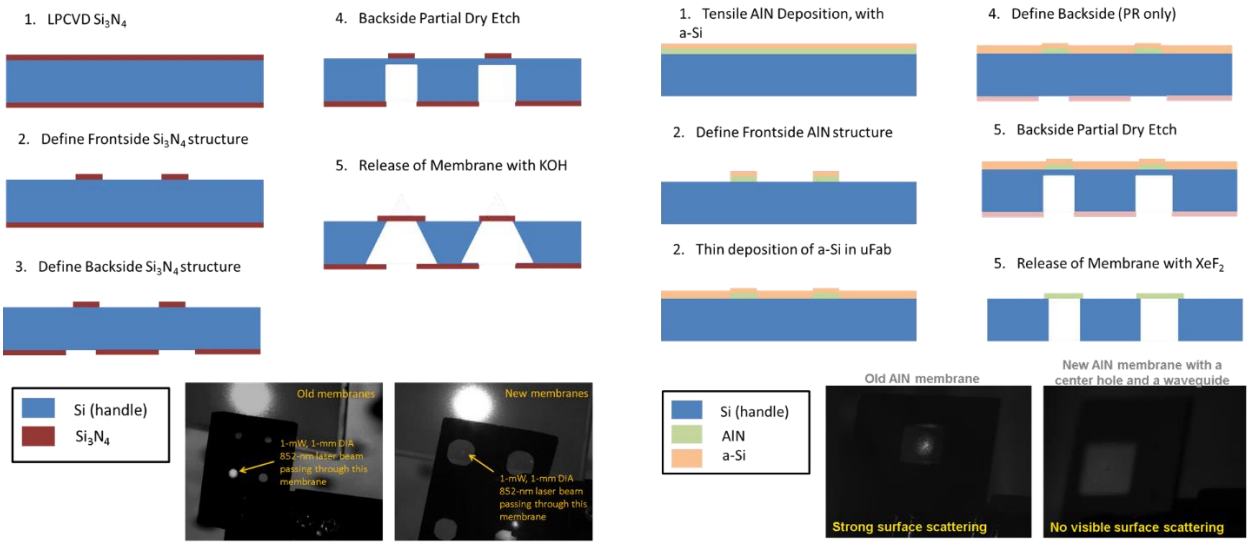

Figure 8. Fabrication of high-quality SiN and AlN suspended membranes

Figure 8 summarizes the latest fabrication flows for making suspended SiN and AlN membranes. The pictures show the improvement of the membrane surface quality comparing the old fabrication process and the latest process. By shining a laser beam through a suspended membrane, we can see obvious surface light scattering from the membranes using an old fabrication procedure but no detectable scattered light from the membranes using the procedures illustrated in Fig. 5. Basically, the major improvement was accomplished by eliminating the use of SiO_2 in the fabrication process.

4.2. Suspended SiN waveguides with free-space optical couplers and photonic crystal reflectors

For early characterization of the suspended waveguides and probing the thermal Cs atom signals via the evanescent field from a waveguide, we fabricated waveguides with photonic-crystal (PC) free-space couplers and PC reflectors. Figure 9 shows an example of the mask pattern of the

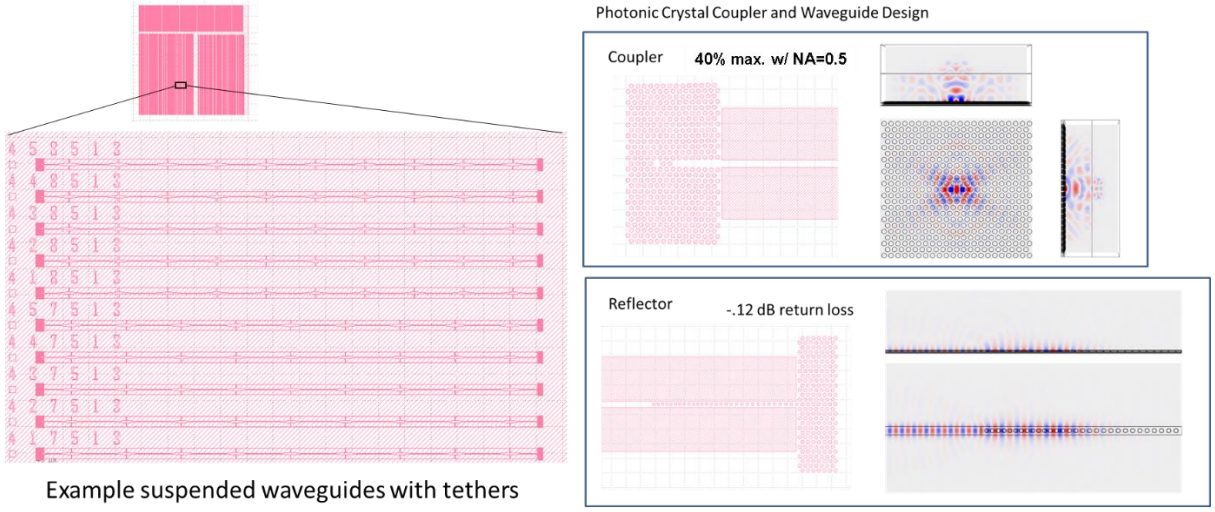

Figure 9. Mask design and simulation of waveguides with PC couplers

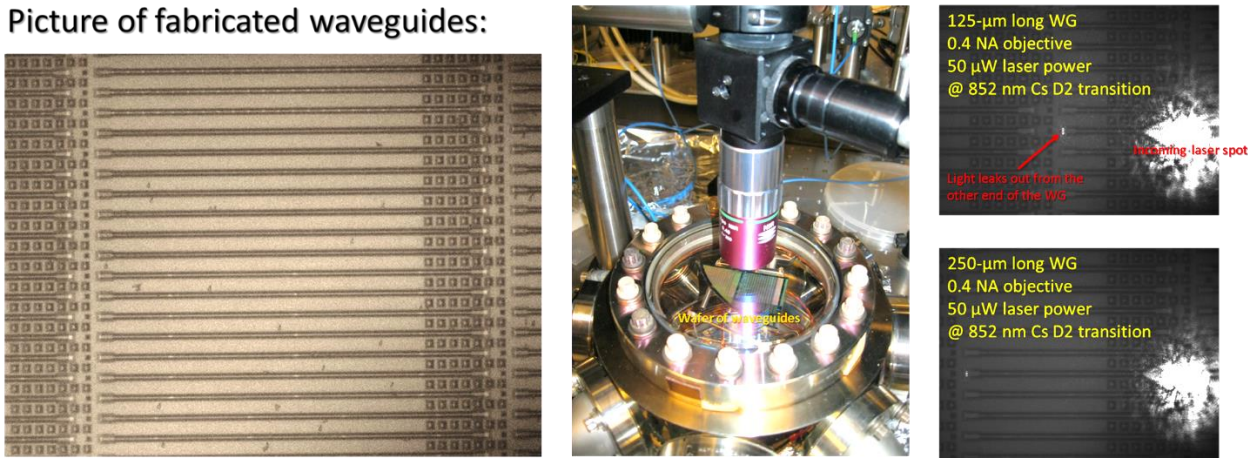

Figure 10. Light coupling into waveguides via PC couplers

waveguide devices from a rectangular area on the wafer and the simulation results of the PC coupler and the PC reflector. Each die contains thousands of waveguides with different lengths and tether configurations. The PC coupler and the PC reflector is designed for 852 nm wavelength, and they are polarization sensitive. Figure 10 displays a picture (on the left) of fabricated 500-μm long waveguides with PC couplers on the right end and the PC reflectors on the left end. The picture at center shows a setup using an NA=0.4 microscope objective lens to couple 852-nm laser into one of the suspended waveguides on a piece of wafer inside a vacuum chamber. The objective lens also serves as an imaging lens for waveguide inspections and light coupling characterization. We have achieved about 20% coupling efficiency through the free-space PC couplers into these SiN waveguides. Limiting by our 852-nm laser source and the experimental implementation, the maximum optical delivered to the waveguides was below 1 mW.

4.3. SiN & AlN suspended waveguides coupled via ATC

Light coupling via a free-space, focusing beam onto a PC coupler and then into a suspended waveguide is usually narrowband in wavelength. To simultaneous couple multiple wavelengths into a waveguide, we fabricated SiN and AlN suspended waveguide devices (WGs) where each WG has a cross-sectional dimension of 500nm x 200 nm and has a 50-μm long taper section and 100 nm taper end. The short taper section is used for an evanescent coupling method, adiabatic transfer coupling (ATC), between a micron-size dimpled fiber and a WG trapper structure. Pictures in Fig.11 demonstrate the experimental pictures of the broadband optical coupling through the ATC method. In the pictures, we can see light (with wavelengths at 937 nm, 852 nm, and 685 nm) is coupled into a waveguide through a dimpled fiber (the curved blurred shadow) and leaking out from the other and of the waveguide. More details are discuss in the Section 5.

4.4. On-going fabrication of the butt-coupling suspended AlN waveguide devices with SiO_2 protection layers

Probably a more reliable fiber coupling technique in fiber optic industry is fiber-to-waveguide

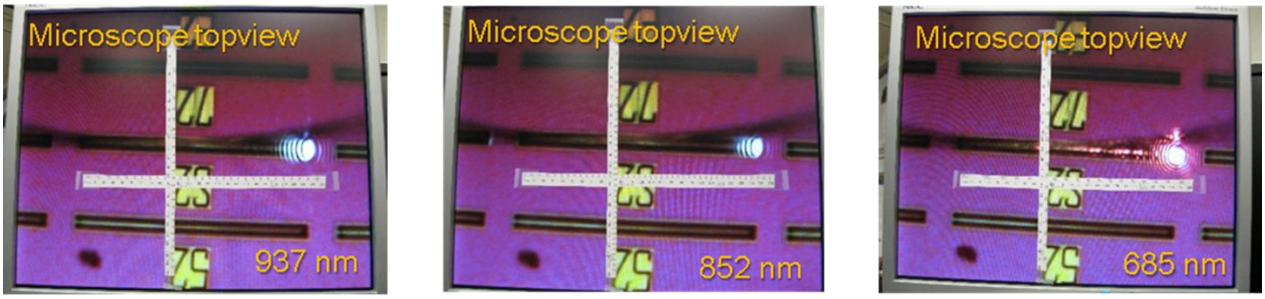

Figure 11. Optical coupling to a WG via ATC

(WG) butt coupling, which matches a fiber mode and a waveguide mode. After light coupling with index matching fluid (UV epoxy), a cleaved fiber is UV-glued on the facet of WGs. The mode field diameter (MFD) of a single mode fiber (780-HP) is 5um@850nm, and the size of an aluminum nitride (AlN) waveguide is about 650nm×200nm. The numerical simulation is illustrated in Fig. 12. Matching two modes, the adiabatic mode conversion requires with an inverse-tapered WG which reduces the dimension of waveguide down to 60nm×200nm and increases the mode of WGs up to 4~5um diameter (MFD) in SiO_2 cladding layer. The inverse-taper-end and linearly inverse-tapered WG are surrounded by both 3um-top and 3um-bottom SiO_2 cladding layer due to the size of a MFD, which is important to hold the inverse-tapered end reliably, achieve a nice WG facet after etching, and have some volume to glue a fiber on. Generally, the fiber-to-WG butt-coupling is robust for in-vacuum application and does not need in-situ light coupling compared to the evanescent-field WG coupling with a dimpled tapered fiber for in-vacuum application.

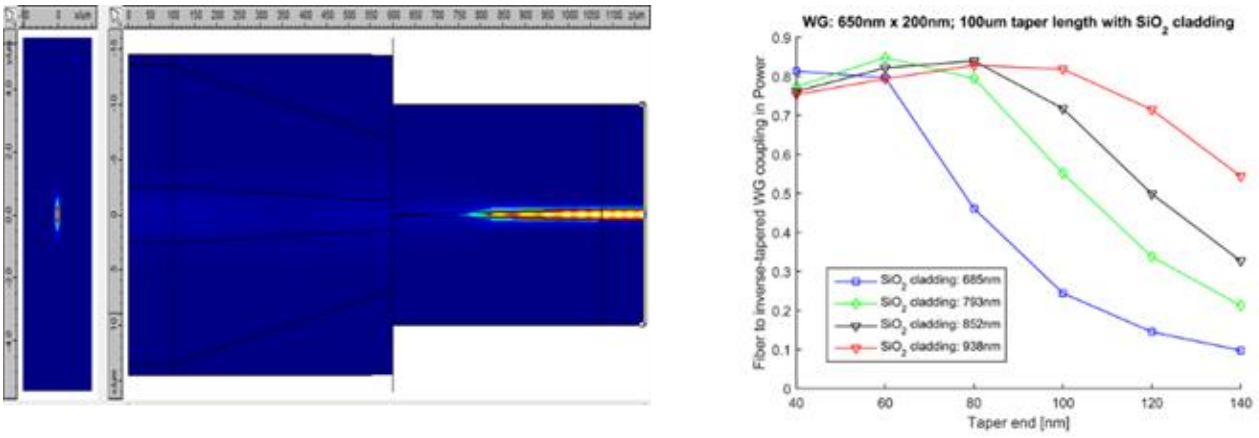

Figure 12. (Left) Mode transferring simulation from a single mode fiber to an inverse-tapered waveguide (60nm taper-end, 100um taper length, WG dimension = 650nm×200nm). (Right) Fiber-to-WG butt-coupling versus the inverse-tapered end for 685nm, 793nm, 852nm, 938nm wavelengths.

A new fiber-to-WG butt-coupling device has ~7.8mm long AlN WG (650nm×200nm) designed for the quasi-TE mode with 200um linearly inverse-tapered WG sections and 60nm inverse-taper-ends. After fiber-to-WG butt-coupling, simple WG transferring process to a vacuum chamber with fixed light coupling makes all the process more convenient and reliable than the evanescent-field coupling with a dimpled tapered fiber.

The detailed fabrication process is described in Fig. 13, and the mask design is illustrated in Fig. 14. The front-side and back-side etching process of a hole and two needle structures for MOT atoms are unique together with AlN WG fabrication, and the process of the etched-through hole is

similar to MEMS process. We considered e-beam lithography for 60nm inverse-taper ends, but we chose photolithography-only fabrication process due to its simplicity, a centimeter-long WG length, and the potential issues of e-beam such as patterning time and stitching errors. Especially, two boundaries of the inverse-tapered WG section are defined by two AlN etching steps. The first AlN etching step defines a bended side edge of inverse-tapered WG sections and etch all the straight WG, and the second AlN etching step defines another bended edge (toward an opposite direction) of inverse-tapered WG sections. The length of inverse-taper is 200um, and the taper-end is 60nm. The 105um-long extended rectangle end (60nm×200nm×105um) with the rectangle anchor (4.6um×200nm×4um) at the end is useful to hold the inverse-tapered end safely during all the fabrication process before dicing process with a dicing saw. The etching process of the dicing on the 105um-long extend rectangle end can also make a nice facet of the inverse-taper-end. Metallic patterned 50um ruler on the inverse-taper-end shows the width of the taper-end and helps to couple the light into the waveguide through the top-view image and fiber back-reflection.

Figure 13. Fabrication process of a fiber-to-WG butt-coupling device with inverse-tapered sections and inverse-taper-ends.

The main sample has a 4.6mm diameter hole with two 300um-wide needle structures which support AlN waveguides across 500um or 750um gap to overlap well with a MOT atoms in the hole. We have produced high atom-number MOTs inside a 4-5mm diameter hole with approximately 500um-1mm gap between two needle structures on the Si substrate with laser cooling and trapping techniques. On the right side of the main sample, there are five testing WGs inside of SiO_2 layer with different lengths (10, 15.2, 19.2, 23.2, 27.2mm), which WGs have

serpentine structures with fiber-to-WG butt coupling geometry for propagation loss measurement and checking aluminum nitride film quality. On the left side of the main sample, there are five testing WGs inside of SiO_2 layer with several inverse-taper-ends (50, 60, 70, 80, 90nm) for checking the optimal fiber-to-WG butt-couplings of 685nm, 852nm, 938nm lights. The inverse-tapered WG section is surrounded by top and bottom SiO2 layers which hold the inverse-taper-end, have a good facet after etching, and offer some volume to glue a cleaved fiber on the facet of WGs with index-matching UV epoxy.

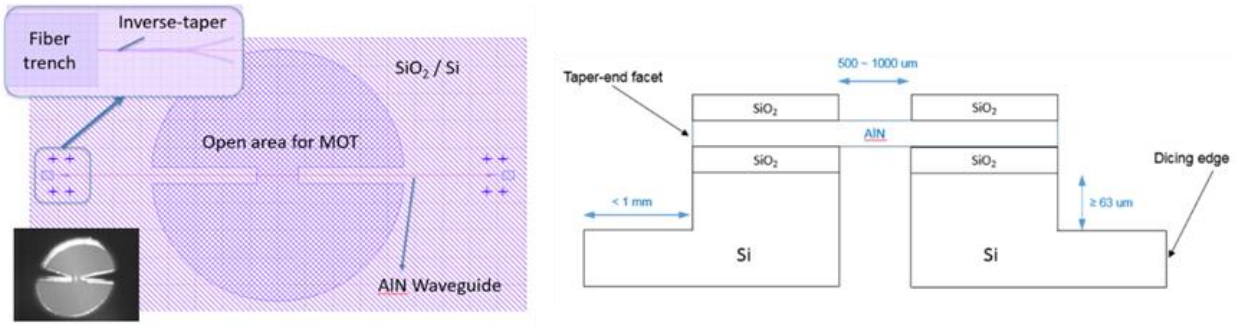

Figure 14. (Left) A new device mask pattern of a fiber-to-WG butt-coupling for atom-light interaction (Left-bottom) MOT in a hole between two needle structure on the Si substrate. (Right) Cross-sectional view of a new fiber-to-WG butt-coupling device for atom-light interaction.

5. Broadband Adiabatic-transfer-coupling (ATC)

A micron-diameter dimpled tapered fiber has been used for the evanescent-field coupling to WG and PC devices [12]. This technique has been widely used in photonic research work, because a dimpled tapered fiber can probe many devices on a sample compared to the butt-coupling technique. The evanescent-field mode of a micron-diameter dimpled tapered fiber has been transferred to the WG mode (500nm×200nm) through a 50μm-long inverse-tapered WG section with a 100nm taper-end. With this short taper structure, we take advantage of the adiabatic transfer effect to realize broadband coupling to the WG. The inverse-tapered WG section and the photonic crystal reflectors were designed by COMSOL simulation for 686nm, 852nm, and 937nm wavelengths (see Fig. 15). The measurement results compared to a simulation curve is plotted on the right in Fig.15.

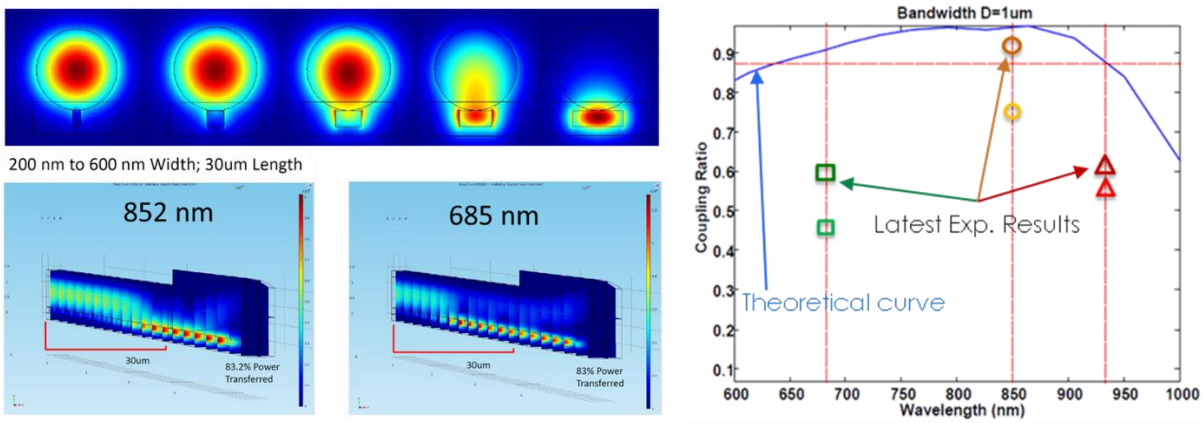

Figure 15. Simulation and experimental results of ATC

The fabrication process of a dimpled tapered fiber is started with a micron-diameter tapered fiber and a molding fiber. For a molding fiber, an unbuffered 125um diameter single mode fiber (780HP) is cleaned by clean room wipes with methanol and held by a rotatable fiber mount. Reducing static surface charges, we spray ionized nitrogen gas on the surfaces of a tapered fiber and a molding fiber with an ionizing gun; this is an important process for taking the molding fiber off from the tapered fiber after molding process. When the tension of a tapered fiber has been relaxed by a step, a molding fiber has been lowered by a step to keep the tension of a V-shaped tapered fiber. We continue this process until 15mm each stretched fiber pulling position becomes 12mm stretched position for both motors, and the symmetry of a V-shaped tapered fiber needs to be balanced by manipulating the position of a molding fiber. For molding a dimpled tapered fiber, a 3mm deep and V-shaped, tensioned tapered fiber is good to start with an instantaneous flame. A long exposure time of H_2 flame on a V-shaped tapered fiber and a molding fiber makes it difficult to detach two fibers after molding process. At the moment of hearing a pop sound, upon initiation

of the H_2 flame, we shut off the H_2 flow. It is expected that a tapered section with more volume than a tapered section with less volume is easier to mold its shape, and a linear-to-exponential tapered fiber would be better than an exponentially tapered fiber for this molding process. After the molding process, the transmission decreases due to its curved shape, and we need to calibrate the evanescent-field WG coupling efficiency based on this.

5.1. Sample probe station

A micron-diameter dimpled tapered fiber held by two fiber holders on two linear motor stages can be used as a sample probe station with horizontal and vertical axes objective lens setup. The WG sample is held by a rotatable fiber mount, and the sample is positioned by precise 3D PZT translation stages (Thorlabs, Nanomax 312D). The dimpled tapered fiber has a 60μm radius dimple within a big U-shaped transition taper, and the side-view of a dimpled fiber shows some different angle between a dimpled part and a big U-shaped part. Therefore, we should rotate the WG sample at the side-view and parallelize it to the overall dimpled tapered fiber to couple the evanescent-field of a small dimpled part to WG without being prevented by the big U-shaped part. The minimum/thinnest section of a dimpled tapered fiber has to be well aligned at the top-view to the WG inverse-tapered section, and the precise 3D PZT translation stage is necessary to position the WG sample. As the sample becomes closer to the dimpled tapered fiber, the surface charges of a WG sample and a fiber interact attractively or repulsively depending on the WG materials together with van der Waals forces. Thus, we need to move the sample closer and wait until the motion of a dimpled fiber is settled down, and it is very helpful to align the fiber well to the WG sample etching edge at the top-view for balancing these forces. When the dimpled fiber is applied to the inverse-tapered section, it adheres well due to van der Waals forces. In addition, the clean-room air flow of a HEPA filter needs to be blocked by a Plexiglas box. The evanescent-field coupling with a dimpled tapered fiber is popular in academia to develop new testing devices because of its ease in accessing multiple devices. However, this is not robust enough for commercial-grade reliable products, whose coupling is based on the fiber-to-waveguide butt-coupling. The transmission of a dimpled tapered fiber decreases because van der Walls forces attract dirt onto the fiber surface. The degradation of a dimpled tapered fiber is decreased in a clean room condition. The touching and detaching of a dimpled tapered fiber on a sample surface actually builds up charges on the fiber surface, which can attract charged particles onto the fiber surface and affect the motion of the fiber, close to the sample. Therefore, discharging the fiber surface with an ionizing gun is essential to reducing charges on the fiber surface. In addition, it is difficult to move the evanescent-field coupled sample. The coupling alignment between an inverse-tapered section of the waveguide and a dimpled tapered fiber is very sensitive. Small vibrations can break the coupling easily. After the evanescent-field coupling at the probe station, we glued the buffered

fiber sections to the two aluminum posts which are anchored on the sample stage, and the coupling is maintained after curing with epoxy. Often, transferring movement can destroy the coupling. Some group successfully glued a tapered fiber to a single photonic device in free space with carbon contamination; a single photonic device has to be detached from the substrate, which seems to be hard to handle. All of our photonic devices have been fabricated on the substrate and are held by tethers. The photonic devices have different waveguide lengths with and without tethers, and multiple-wavelengths photonic crystal reflectors have been integrated with an inverse-tapered waveguide section for 685nm, 852nm, and 938nm. Therefore, we can measure the level of reflected light through a circulator. The simple fabrication process is as follow: aluminum nitride (or silicon nitride) is deposited on silicon substrate. Waveguides with photonic crystal reflectors and inverse-tapers are patterned and dry-etched. The photonic devices with tethers on silicon substrate are released from silicon substrate with wet etching process. The evanescent-field coupling for a short waveguide is reliably worked well with PZT 3D stages. For a long waveguide (>100μm), there was lower transmission issue due to film quality and e-beam stitching errors.

5.2. Evanescent-field coupling to the waveguide in vacuum

The evanescent-field coupling with a dimpled tapered fiber in vacuum is challenging due to imaging issues, the sample manipulation issues, and the difficulty of removing static charges. The working distance of an objective lens (Mitutoyo 10x M Plan APO, NA = 0.28) is about 33.5mm, and the sample with a dimple fiber needs to be installed close to a 5mm-thick glass window on the top of a vacuum chamber. There is no room to set up a horizontal-view objective lens. We tried to set up an angle-view objective lens, but it is difficult to get a good image due to surface scattered photons from the optical window (see Fig.16). Instead, we set up a 3mm×3mm 45-angled mirror

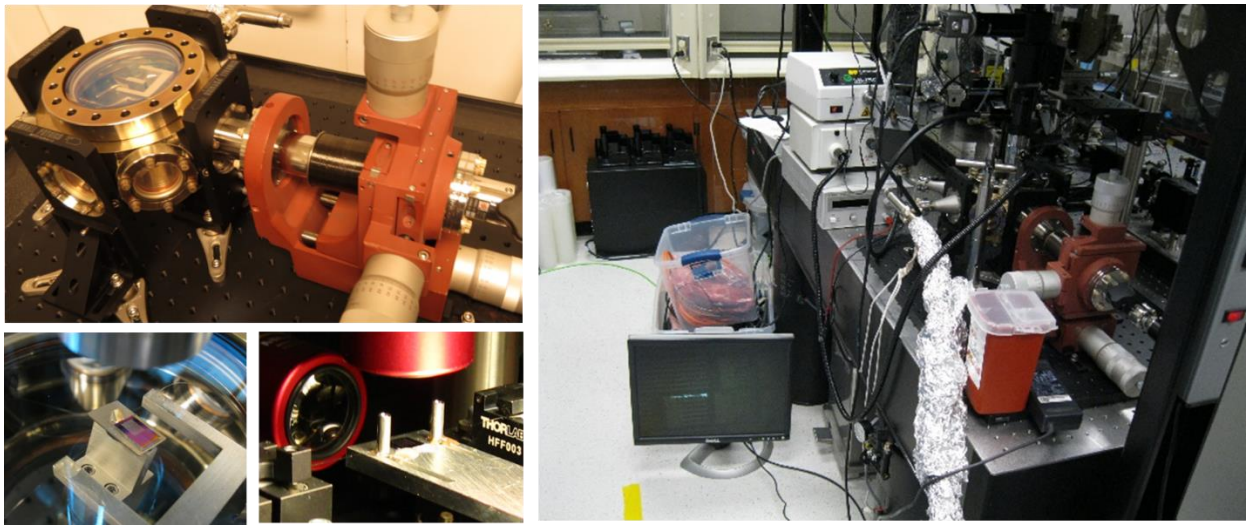

Figure 16. Apparatus for ATC to the waveguide in vacuum

on the sample holder to see the side-view through a vertical objective lens. In addition, using a 780-nm LED (Thorlabs, 20nm broad) light also helps to improve the image without creating interference patterns. Because of the geometry of a dimpled tapered fiber, the sample must be well aligned to the fiber along the side-view. A big U-shaped transition taper of a dimpled fiber has some angle, and the sample carrier of a waveguide sample has to be rotated by the rod of a 3D vacuum manipulator. The waveguide sample on a stainless-steel sample carrier is fixed to a magnet attached to the rod of a vacuum manipulator. This configuration allows adjustment of the waveguide sample relative to the micron-diameter tapered fiber along the top-view image. Sometimes, the fabricated tapered fiber is slightly twisted, and there is some difference between the micron-diameter tapered fiber and the transition tapers. Surface charge, on the etch-through boundaries of the silicon substrate near the waveguide, affects the motion of a dimpled tapered fiber by attractive/repulsive force. Alignment of the tapered fiber using the top-view with a vacuum manipulator lessens fiber motion when the dimpled fiber becomes closer to the waveguide sample. The vacuum manipulator is controlled by a manual translation stage, and its minimum resolution is 2μm. It is difficult to control the sample compared to 3D PZT translation stages. In addition, the one-axis motion of this 3D manual vacuum manipulator causes two axes to wobble, because the sample stage is connected to the rod end and the transition plate is connected to the rod middle. In vacuum (2×10^{-7}torr), there is no buffer gas and we cannot use an ionizing gun, thus charging issues become more severe. For the aluminum nitride waveguide, we coupled ~450μW optical power into the waveguide in vacuum and to test the power capacity of aluminum nitride, which is ten times more thermal conductivity than silicon nitride. We used a turbo pump to attain this vacuum.

6. Evanescent-field photon-atom interactions

We used the sub-micron diameter section of a tapered fiber and a suspended waveguide with free-space PC coupler to detect the thermal Cs atom signal inside a vacuum chamber. This helped us verify if the nanofiber or the microfabricated waveguide can provide enough extension of the evanescent field. The Cs vapor was produced by using either a Cs getter or a Cs ampule.

6.1. Probe free-space atom signal via an optical nanofiber

We mounted one of the pulled tapered fibers inside a vacuum chamber. The sub-micron diameter section ran across the two stands of a U-shape mount by gluing the buffered optical fiber (the part before the fiber was tapered down) on the two stands. The vacuum chamber was connected to a Cs ampule. By heating up the chamber and the ampule temperature, we can control the Cs vapor density inside the chamber. Figure 17 shows the measured Cs atom signal as the red curve using the nanofiber at the chamber temperature of 106ºC comparing to the saturation spectroscopy signal (blue curve) from a room-temperature Cs vapor cell. For this measurement, we used 894-nm laser light to probe the Cs $D1$ transition. As we can see, the $D1$ optical resonance linewidth of Cs atoms is broader than the Doppler width at the same temperature. This is ascribed to the fact that the atom transit time through the evanescent-field region is very short and causes this additional linewidth broadening. Hence, measuring the atomic optical resonance linewidth can reveal some information regarding the size of the evanescent field.

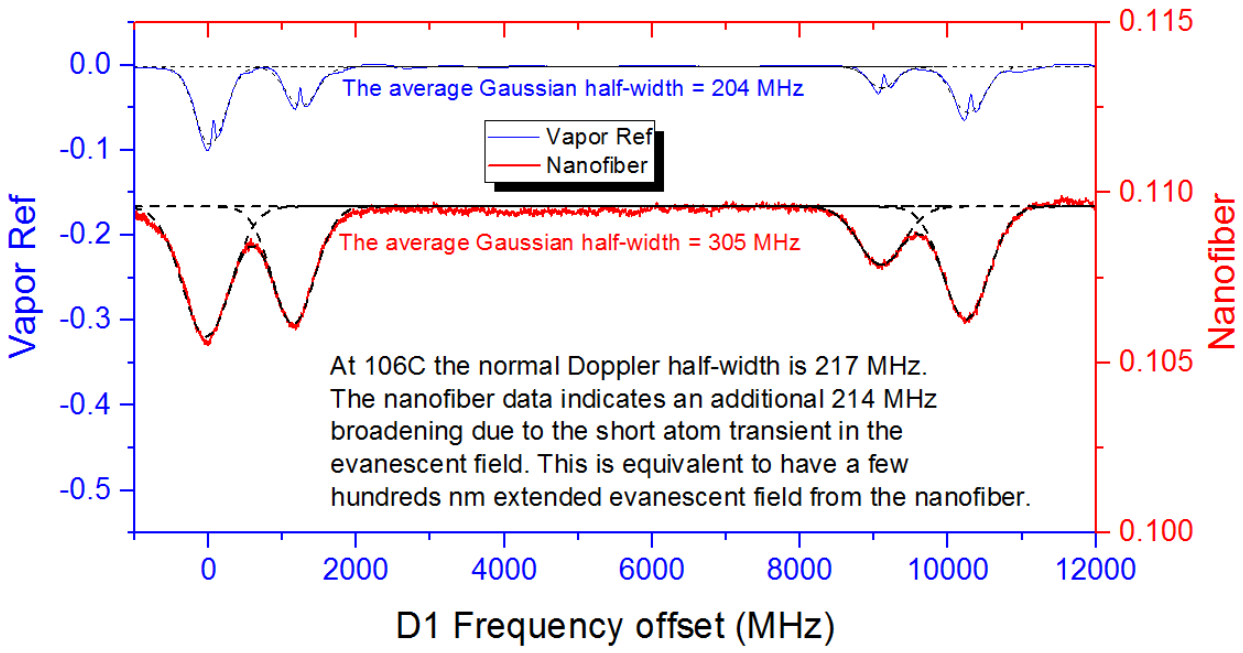

Figure 17. Nanofiber detected thermal Cs atom signal

6.2. Probe free-space atom signal via a microfabricated suspended waveguide

For detecting the Cs atom signal using a suspended waveguide, we took advantage of fabricated SiN waveguides (500 nm x 200 nm x 125 µm, 250 µm, 500 µm, 1000 µm) with PC couplers and PC reflectors. As shown in Fig. 18, a cleaved piece of the SiN waveguide wafer was placed inside a vacuum chamber. In the IR viewing image, we can see the glowing laser beams and the Cs dispenser (Cs getter) owing to the fact that the chamber was filled with Cs vapor. We later attached a Cs ampule to the chamber to obtain more Cs vapor density.

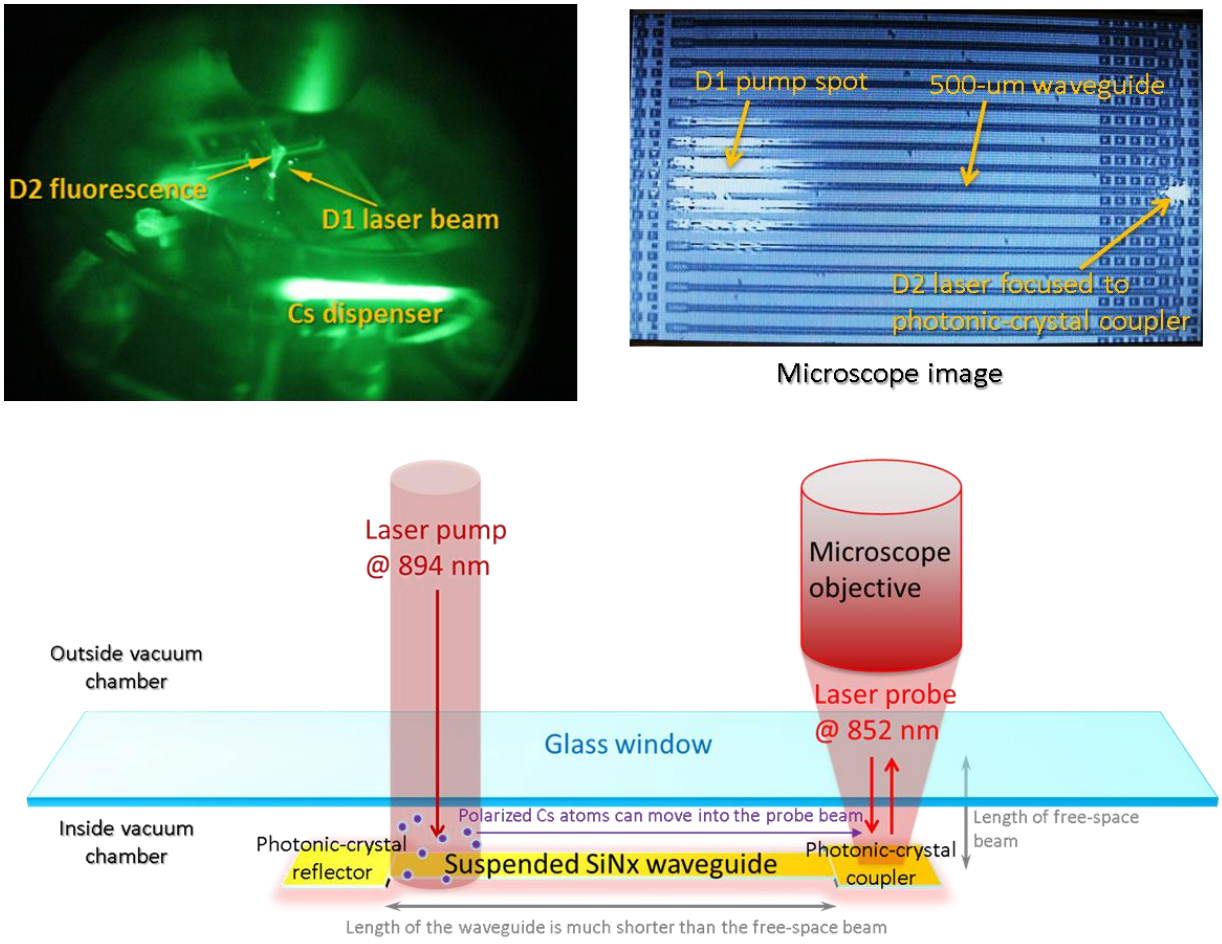

Figure 18. Experimental illustration of the waveguide detected Cs atom signal

Because of the way we couple the probe light into the waveguide, we use the following method to probe the atom signal. The probe beam is tuned on *D*2 Cs resonance, which is associated with the same ground-state hyperfine manifold as the pump laser. The *D*1 pump laser is used to polarize Cs atoms by doing hyperfine optical pumping, which depletes the population in the associated hyperfine manifold. Therefore, the polarized atoms do not attenuate the probe light. Ideally, the probe laser is guided by the waveguide and its evanescent field can be used to detect polarized

atoms. However, both the waveguide evanescent field and the probe beam propagating through free space can see polarized atoms. Since there is a finite distance between the suspended waveguide and the chamber glass window, the polarized Cs atoms can move between the pump beam volume and the probe beam volume and contribute to the probe signal.

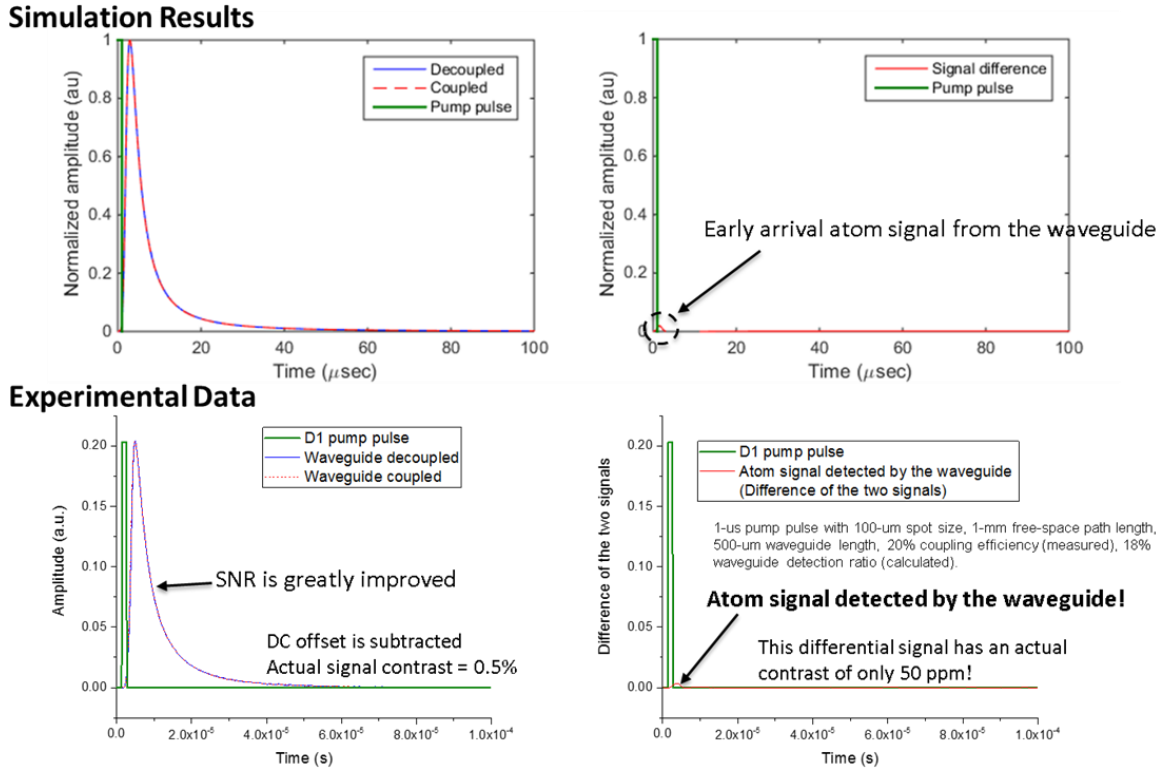

Figure 19. Modeling simulation and experimental results

By pulsing the pump laser, we can detect the time-dependent response in the probe signal. Because the waveguide detected signal arrives earlier (speed of light in the waveguide) than the free-space atom transporting signal (thermal atom speed), we are able to demonstrate the waveguide probed atom signal by taking the difference of the probed atoms signal with WG coupled and WG decoupled. Figure 19 shows the experimental result that matches very well with the modeling simulation. The experimental data is consistent with the calculated atom signal probed by the evanescent field produced by the designed waveguide.

7. Cold atom production at the waveguide

Production of cold atoms with constant atomic cooling force at the waveguide atom traps is important to efficiently load atoms into a relatively weak evanescent-field trapping potential. A normal scheme to cool and trap atoms at a specific location is to make a MOT. Due to its cooling and trapping mechanism, MOTs are more capable of collecting atoms with large laser beams as experimentally verified in Ref.[13]. The trapped atom number is scaled by $d^{3.6—6}$, where d is the MOT beam diameter. This makes an unfavorable condition for producing a MOT cloud at a microfabricated suspended waveguide, which is usually with a length ≤ 1 mm, and therefore the effective beam diameter to be used is smaller than 1 mm. The atom number in the MOT is very low under this condition. On the contrary, a nanofiber pulled from a normal single-mode fiber can be as long as a few mm to 1 cm. Large MOT laser beams can be used to produce a high number cold atom cloud at the nanofiber with a sub-Doppler cooling scheme to efficiently load atoms into the nanofiber traps.

We have explored two major approaches to achieve this goal. The basic idea is to keep utilizing a large MOT beam for large capture volume and concentrate the atoms into the MOT trapping center at a small opening gap for the suspended waveguide. One is to use a silicon needle structure to allow most of the MOT beams to pass through a larger silicon hole but produce a concentrated MOT cloud inside the needle gap, which can have a suspended waveguide running across it. The other approach is to use a high quality SiN or AlN suspended membrane with a nano-waveguide running across a small hole at the center. A transparent membrane virtually cannot be seen by the MOT beams and therefore enables large capture volume. The details of this work will be described in Ref.[14]. Figure 20 illustrates the simulation and experimental results of producing a high atom number MOT cloud inside a few hundred microns membrane hole with a nano-waveguide.

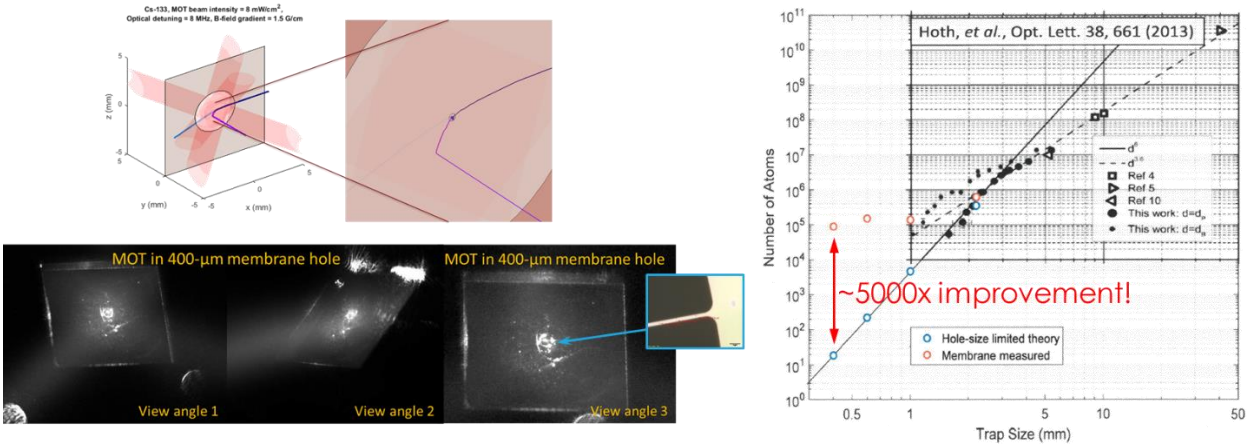

Figure 20. High atom number MOT inside a sub-millimeter hole

8. High-degree spin squeezing with a square waveguide

Through theoretical studies, we have identified that a square-like waveguide (SWG) can actually be utilized for generating atomic spin squeezed state with a better performance than using a circular waveguide, such as a nanofiber. Figure 21 summarizes the preliminary study results assuming there are 2500 Cs atoms participating in the spin squeezing protocols. One can see the significant improvement by using an SWG compared to a nanofiber. The details of this work will be described in Ref.[15].

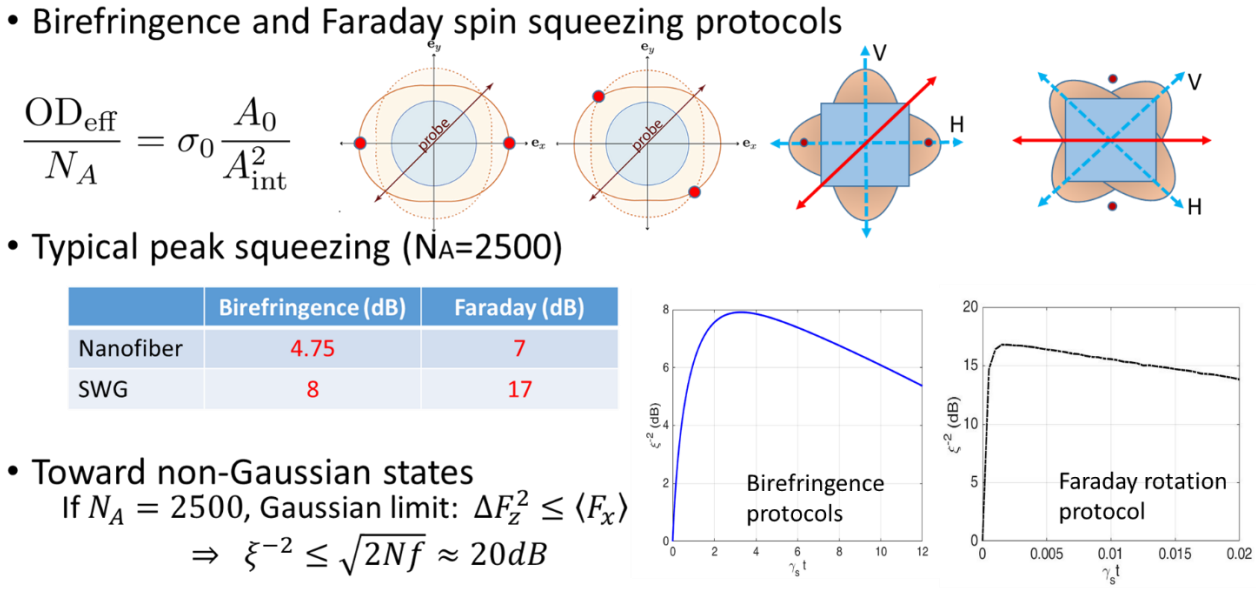

Figure 21. High-degree spin squeezing using a square WG

9. Summary & Outlook

Throughout this research project, we have established modeling capabilities including photonic-crystal waveguide modeling, WG associated atomic-physics modeling, modeling for WG-assisted atomic spin squeezing. We have developed two tapered-fiber pulling systems for making micron-size dimpled fibers and high-optical-transmission sub-micron linear-to-exponential tapered fibers. We have carried out and developed various fabrication processes for SiN and AlN waveguide fabrications. The fabrication work of suspended AlN waveguides with SiO_2-protected inverse taper structure has potential to overcome the problems with SiN waveguides seen by several groups. Our accomplishments are the essential elements that will help future photonic AMO projects at Sandia and finally moving toward the alignment-free on-chip neutral-atom quantum controls.

REFERENCES

1. A. H. Barnett, S. P. Smith, M. Olshanii, K. S. Johnson, A. W. Adams, and M. Prentiss, "Substrate-based atom waveguide using guided two-color evanescent light fields," Phys. Rev. A **61**, 023608 (2000).

2. James P. Burke, Jr., Sai-Tak Chu, Garnett W. Bryant, C. J. Williams, and P. S. Julienne, "Designing neutral-atom nanotraps with integrated optical waveguides," Phys. Rev. A **65**, 043411 (2002).

3. E. Vetsch, D. Reitz, G. Sague, R. Schmidt, S. T. Dawkins, and A. Rauschenbeutel, "Optical Interface Created by Laser-Cooled Atoms Trapped in the Evanescent Field Surrounding an Optical Nanofiber," Phys. Rev. Lett. **104**, 203603 (2010).

4. A. Goban, K. S. Choi, D. J. Alton, D. Ding, C. Lacroute, M. Pototschnig, T. Thiele,1,N. P. Stern, and H. J. Kimble, "Demonstration of a State-Insensitive, Compensated Nanofiber Trap," Phys. Rev. Lett. **109**, 033603 (2012).

5. Chang, D. E., Cirac, J. I., Kimble, H. J., "Self-Organization of Atoms along a Nanophotonic Waveguide," Phys. Rev. Lett. **110**, 113606 (2013).

6. Lee, J., Park, D. H., Mittal, S., Dagenais, M., Rolston, S. L., "Integrated optical dipole trap for cold neutral atoms with an optical waveguide coupler," New J. Phys. **15**, 043010 (2013).

7. C.-L. Hung, Alejandro González-Tudela, J. Ignacio Cirac, and H. J. Kimble, "Quantum spin dynamics with pairwise-tunable, long-range interactions," Proc. Natl. Acad. Sci. **113**, E4946-E4955 (2016).

8. J. D. Thompson, T. G. Tiecke, N. P. de Leon, J. Feist, A. V. Akimov, M. Gullans, A. S. Zibrov, V. Vuletić, M. D. Lukin, "Coupling a Single Trapped Atom to a Nanoscale Optical Cavity," Science **340**, 1202 (2013).

9. A. Goban, C.-L. Hung, J. D. Hood, S.-P. Yu, J. A. Muniz, O. Painter, and H. J. Kimble, "Superradiance for Atoms Trapped along a Photonic Crystal Waveguide," Phys. Rev. Lett. **115**, 063601 (2015).

10. W. Happer, Y.-Y. Jau, and T. Walker, "Optically Pumped Atoms," Wiley-VCH (2010).

11. J. E. Hoffman, S. Ravets, J. A. Grover, P. Solano, P. R. Kordell, J. D. Wong-Campos, L. A. Orozco, and S. L. Rolston, "Ultrahigh transmission optical nanofibers," AIP Advance **4**, 067124 (2014).

12. Simon Groblacher, Jeff T. Hill, Amir H. Safavi-Naeini, Jasper Chan, and Oskar Painter, "Highly efficient coupling from an optical fiber to a nanoscale silicon optomechanical cavity," Appl. Phys. Lett. **103**, 181104 (2013).

13. Gregory W. Hoth, Elizabeth A. Donley, and John Kitching, "Atom number in magneto-optic traps with millimeter scale laser beams," Opt. Lett. **38**, 661 (2013).

14. G. Biedermann, J. Lee, J. Mudrick, E. Douglas, and Y.-Y. Jau, "Cold-atom production for SiN and AlN microstructures," in preparation for Opt. Lett.

15. X. Qi, I. Deutsch, and Y.-Y. Jau, "Strong spin squeezing using microfabricated square waveguides," in preparation for Phys. Rev. A.

DISTRIBUTION

4 Lawrence Livermore National Laboratory
Attn: N. Dunipace (1)
P.O. Box 808, MS L-795
Livermore, CA 94551-0808

1	MSXXXX	Name of Person	Org. Number
1	MSXXXX	Name of Person	Org. Number
1	MS0899	Technical Library	9536 (electronic copy)

For LDRD reports, add:

1	MS0359	D. Chavez, LDRD Office	1911

For CRADA reports add:

1	MS0115	OFA/NFE Agreements	10012

For Patent Caution reports, add:

1	MS0161	Legal Technology Transfer Center	11500


Sandia National Laboratories